Solid-state disordering and melting of silica stishovite: the role of defects

2006 J. Phys.: Condens. Matter 18 659

(http://iopscience.iop.org/0953-8984/18/2/021)

INSTITUTE OF PHYSICS PUBLISHING JOURNAL OF PHYSICS: CONDENSED MATTER

J. Phys.: Condens. Matter **18** (2006) 659–668 doi:10.1088/0953-8984/18/2/021

Solid-state disordering and melting of silica stishovite: the role of defects

Sheng-Nian Luo[1,4], **Lianqing Zheng**[2] **and Oliver Tschauner**[3]

[1] P-24 Plasma Physics, Los Alamos National Laboratory, Los Alamos, NM 87544, USA
[2] Department of Chemistry, University of Missouri, Columbia, MO 65211, USA
[3] High-Pressure Science and Engineering Center and Department of Physics, University of Nevada, Las Vegas, NV 89154, USA

E-mail: sluo@lanl.gov (Sheng-Nian Luo)

Received 13 September 2005, in final form 9 November 2005
Published 14 December 2005
Online at stacks.iop.org/JPhysCM/18/659

Abstract

Molecular dynamics simulations are conducted to investigate disordering of stishovite (a high-pressure polymorph of silica) and the role of defects including grain boundaries, vacancies and free surfaces. It is shown that pre-existent defects initiate or facilitate solid-state disordering and melting. As illustrated in the case of vacancies, melting precedes solid-state disordering for stishovite with low defect concentrations, while defect-rich stishovite may transform into high-density vitreous silica which then undergoes a (quasi-)continuous transition into melt. In sharp contrast, melting of ordinary glass at the same heating rate is sluggish yet evidently first order. Disordering on free surfaces is anisotropic, being more pronounced on (101), (011) and (111) than on (100), (010), (001) and (110) crystallographic planes.

(Some figures in this article are in colour only in the electronic version)

1. Introduction

Stishovite, a high-pressure polymorph of silica with sixfold coordinated Si atoms, is of long-lasting interest in condensed matter physics, geophysics and planetary sciences and for its potential engineering applications [1–9]. At ambient conditions, stishovite is metastable relative to α-quartz with an excess Gibbs free energy [10] of 53.46 kJ mol^{-1}; however, micron-grain-sized polycrystalline stishovite synthesized in high-pressure presses [7] and from natural impacts [11] may remain structurally ordered over geological timescales. Stishovite structure can be preserved even with moderate heating at ambient pressure: it becomes disordered without melting at 500–850 °C in experiments [2, 9, 12]. Previous experimental and computational efforts have mostly focused on changes upon compression of low-density

[4] Author to whom any correspondence should be addressed.

tetrahedral silica (e.g. [3, 13–17]). It is our intention here to examine disordering of high-density silica stishovite at low pressures (ambient and zero). Some particularly interesting issues are the detailed structure evolution upon heating, disordering mechanisms, the effect of defects, and the relationship between solid-state disordering and melting. Nonetheless, these issues have rarely been explored.

Previous Brillouin and Raman scattering experiments [9] have suggested that solid-state disordering in stishovite is not induced, or at least not triggered, by softening of a bulk phonon, and that disordering depends on crystallographic orientations. Recently, spontaneous disordering of nanometre-grain-sized polycrystals and clusters observed in molecular dynamics (MD) simulations indicates the important role of defects in stishovite disordering [18]. MD simulations have been extensively conducted on the silica system to investigate, for example, solid-state amorphization of quartz, densification of glass and high-pressure melting of stishovite [13–15, 19, 20]. In this work, we explored the disordering process of defective stishovite at high temperatures and ambient (or zero) pressure using MD simulations, including solid-state disordering and melting, and disordering anisotropy. The defects investigated include grain boundaries, vacancies and free surfaces, and play a key role in the disordering process of stishovite.

2. Molecular dynamics simulations

The interactions between atoms i and j ($i, j \in \{\mathrm{Si}, \mathrm{O}\}$) separated by a distance of r_{ij} and with charges respectively of q_i and q_j were described by the widely used pairwise van Beest–Kramer–van Santen (BKS) silica potential [21] with a 30–6 Lennard-Jones correction [22]:

$$U_{ij} = \frac{q_i q_j}{4\pi\epsilon r_{ij}} + A_{ij}\mathrm{e}^{-B_{ij}r_{ij}} - \frac{C_{ij}}{r_{ij}^6} + 4\epsilon_{ij}\left[\left(\frac{\sigma_{ij}}{r_{ij}}\right)^{30} - \left(\frac{\sigma_{ij}}{r_{ij}}\right)^{6}\right], \tag{1}$$

where A_{ij}, B_{ij}, C_{ij}, ϵ_{ij} and σ_{ij} are parameters and ϵ is the dielectric permittivity constant. The long-range Coulombic term was calculated by the smooth particle mesh Ewald method [23]. The linked-list method [24] was used for computing short-range interactions with a cut-off distance of 1 nm. Long-range corrections for the total potential energy and stress tensor due to cut-off in short-range terms were also included [25].

The defects considered here (figure 1) include grain boundaries in nanometre-grain-sized polycrystals (nanocrystals), vacancies and free surfaces (clusters). Nanocrystals with N_g grains were constructed using the Voronoi scheme [18, 26, 27] from $12 \times 12 \times 20$ and $24 \times 24 \times 40$ supercells. The average grain size is defined as $d_\mathrm{g} \equiv (V/N_\mathrm{g})^{1/3}$, where V is the volume of the simulation cell. Vacancy normally refers to a missing atom. However, for electrical neutrality of the silica system simulated, we chose to randomly remove a single SiO_2 unit from a $6\times6\times10$ supercell (720 SiO_2 units), forming a small three-vacancy cluster, which is referred to as a vacancy for simplicity in the following discussions. N_v SiO_2 units were randomly removed to create N_v vacancies. Free surface was simply the sphere enclosing a cluster of 5 nm diameter and 2871 SiO_2 units. To investigate the anisotropy of the disordering, we constructed semi-clusters by cutting the whole 5 nm cluster along distinctly different crystallographic planes. For comparison, we also conducted simulations on glass. A continuous random network of glass with 502 SiO_2 units was constructed using the Vink–Barkema algorithm [28]. The ambient density is 2.29 and 4.35 g cm^{-3} for glass and stishovite, respectively.

In MD simulations, we adopted the isothermal–isostress ensemble except for clusters (the isothermal–isochoric ensemble was used instead). Nosé thermostat and Parrinello–Rahman barostat were used respectively for temperature and pressure controls [29, 30].

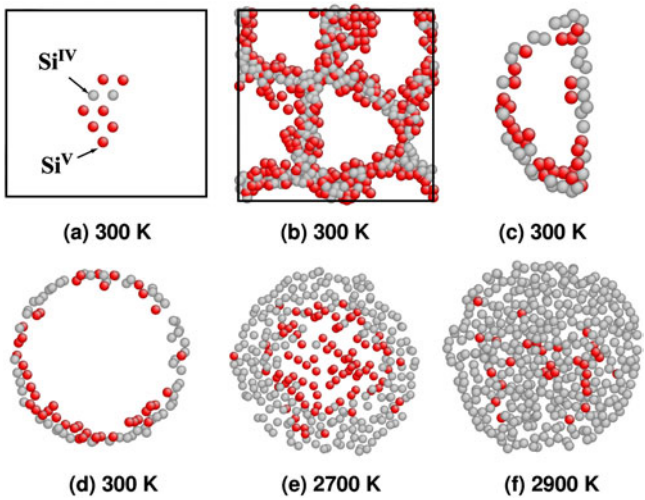

Figure 1. Representative stishovite structures with various defects. Only four- and fivefold coordinated Si atoms (Si^{IV} and Si^{V}) are shown, and empty space represents atoms in stishovite structure (e.g., Si^{VI}). Models equilibrated at 300 K: vacancies (a), grain boundaries in a nanometre-grain-sized polycrystal (b) and free surfaces on a semi-cluster (c) and a whole cluster (d). As an example, (e) and (f) demonstrate disordering of a cluster upon heating. Visualization adopted AtomEye [27].

Three-dimensional periodic boundary conditions were applied in all the simulations. In the case of a cluster, the cluster was centred in a cubic supercell with edge lengths significantly larger than the cluster size and the cut-off distance. Thus the interaction between neighbouring clusters can be neglected, yielding effectively an isolated cluster in vacuum. While the cell volume was preserved under an isothermal–isochoric ensemble, the cluster was not constrained, and its shape and volume were allowed to change. The corresponding stresses were zero on average. The Voronoi nanocrystals were first equilibrated using a time step of 0.01 fs followed by successively larger steps of 0.1–3 fs. We used time steps of 0.5–1 fs for other configurations. Simulation durations varied from 50 to 600 ps.

The static structure properties were characterized by the radial distribution function $g(r)$ (RDF), static structure factor $S(q)$, bond-angle distribution (BAD) and Si-ring-size distribution. In a polyatomic system, the RDF of atom type α and type β is [31]

$$g_{\alpha\beta}(r) = \frac{3V\langle n_{\alpha\beta}(r)\rangle}{4\pi N_\alpha N_\beta[(r+\Delta r)^3 - r^3]}, \tag{2}$$

where N_α and N_β are the number of atoms respectively for type α and β, and $N = N_\alpha + N_\beta$; $n_{\alpha\beta}(r)$ is the number of atoms of type β in a shell between r and $r + \Delta r$ around an atom of type α. The static structure factor can be calculated from $g_{\alpha\beta}$ as

$$S_{\alpha\beta}(q) = \delta_{\alpha\beta} + 4\pi\rho(c_\alpha c_\beta)^{1/2}\int_0^{r_{\max}} r^2[g_{\alpha\beta}(r) - 1]\frac{\sin(qr)}{qr}\frac{\sin(\pi r/r_{\max})}{\pi r/r_{\max}}\mathrm{d}r, \tag{3}$$

where q is the scattering factor, $c_\alpha = N_\alpha/N$, and the number density $\rho = N/V$. The neutron scattering structure factor [32] follows as

$$S_{\mathrm{N}}(q) = \frac{\sum_{\alpha\beta} b_\alpha b_\beta (c_\alpha c_\beta)^{1/2}[S_{\alpha\beta}(q) - \delta_{\alpha\beta} + (c_\alpha c_\beta)^{1/2}]}{(\sum_\alpha b_\alpha c_\alpha)^2}, \tag{4}$$

where b_α is the coherent neutron scattering length of atom type α. ($b_{\mathrm{Si}} = 4.149 \times 10^{-15}$ m and $b_{\mathrm{O}} = 5.803 \times 10^{-15}$ m [33].)

We also calculated the bond-angle distribution (BAD) and ring-size distribution. For BAD, we built up a list of nearest neighbours (defined by RDF) for Si–Si, Si–O and O–O pairs, and bond angles were then calculated for each atom relative to its neighbours. The ring structure is characteristic of the topology of silica phases. A ring is a closed path consisting of Si–O bonds, and its size is represented by the number of Si atoms in the ring: an n-member ring contains n Si and $2n$ O atoms. The ring-size distribution is a statistical distribution of the number of rings around a Si atom, and was calculated following Yuan and Cormack [34].

The average diffusion coefficient (D) was calculated from the integrated velocity autocorrelation function using the Green–Kubo expression [24]:

$$D = \frac{1}{3N}\int_0^\infty \left\langle \sum_{j=1}^{N} \mathbf{v}_j(t)\cdot\mathbf{v}_j(0)\right\rangle \mathrm{d}t, \tag{5}$$

where t denotes time and $\mathbf{v}$ velocity. D can be useful to distinguish a crystalline or disordered solid (including glass) from liquid: D of liquid can be higher by one to three orders of magnitude.

3. Results and discussion

We first examined a defect-free stishovite crystal (without free surfaces or other defects) subjected to incremental heating at ambient pressure. Temperature was increased successively from 300 K with an increment of 200 K. The system was equilibrated for 50 ps at each temperature, and thermalization was achieved within the first few picoseconds. During incremental heating up to 4500 K, its density decreases steadily and then drops dramatically (by ∼31%) at 4700 K, indicating a first-order phase transition (figure 2). The atomic configuration at 4700 K is highly disordered as seen from the RDF and atomic visualization; thus the phase change can be solid-state disordering or melting. The average diffusion coefficient D is on the order of 10^{-12} m^2 s^{-1} at 4500 K while it increases to 10^{-9} m^2 s^{-1} at 4700 K (figure 3). The latter value is close to those of the melts formed from glass and defective stishovite at the same temperature (figure 3). On the other hand, D of a disordered solid is expected to be comparable to its crystalline counterpart. Thus, a defect-free stishovite crystal melts without solid-state disordering, but with density reduction mostly due to the Si-to-O coordination number reduction from 6 to 4. Similar behaviour has also been observed for stishovite described by the Tsuneyuki potential [9]. (The defect-free stishovite may have been superheated [35, 36]; however, as stishovite is metastable at ambient pressure, the equilibrium melting point and superheating are not well defined.) This implies that solid-state disordering of stishovite certainly requires sufficient concentration of defects such as grain boundaries, vacancies and free surfaces.

Grain boundaries are two-dimensional interfaces between neighbouring grains in random crystallographic orientations, accompanied by bond breaking, local disordering and enhanced free energy. We have examined previously the spontaneous disordering of nanocrystalline stishovite [18] at ambient conditions and found that the extent of spontaneous disordering increases with decreasing grain sizes, i.e., with increasing percentage of defective atoms at grain boundaries. As the relevant details as regards the effect of grain boundaries were reported elsewhere [18], we focus below on vacancies and free surfaces.

3.1. Vacancies

MD simulations were conducted on defective structures with 1, 2, 10, 20, 50 and 100 random vacancies out of 720 SiO_2 units (c_v varying from 0 to 0.14), which were subjected to incremental heating under constant-temperature–constant-stress ensemble at ambient pressure

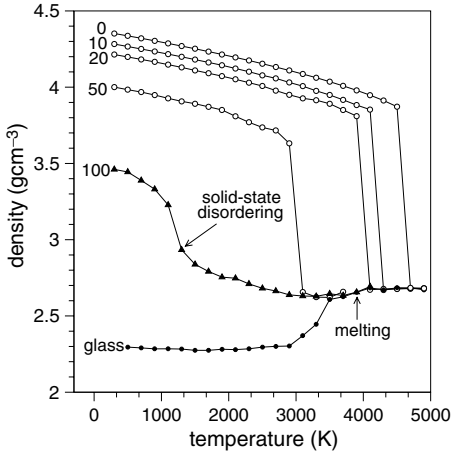

Figure 2. Solid-state disordering and melting of stishovite with various concentrations of vacancies, in comparison with melting of glass: density versus temperature. Numbers denote the numbers of SiO_2 units randomly removed from a supercell of 720 SiO_2 units.

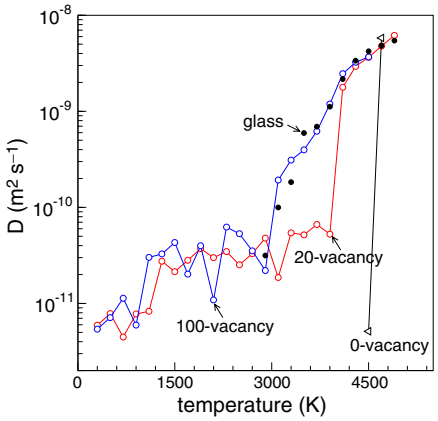

Figure 3. Diffusion coefficient versus temperature for stishovite with various concentration of vacancies and for glass.

(figures 2–5). For comparison, we also performed similar simulations on silica glass, and incremental cooling of silica liquid at the same rate (4 K s^{-1}).

Incrementally heated stishovite structures with 1, 2, 10, 20 and 50 vacancies behave similarly to the defect-free one: density decreases gradually prior to the phase transition, where dramatic density decrease occurs (figure 2). While the phase transition temperature is the same within uncertainties (4700 K) for zero, one and two vacancies, substantial increase in c_v induces its reduction to 4300, 4100 and 3100 K, respectively for 10, 20 and 50 vacancies. In the case of 100 vacancies, however, the density decrease is pronounced between 500 and 1300 K and continues slowly to 2900 K. We may identify a phase transition temperature of 1300 K from the density change as in the cases of 0, 1, 2, 10, 20 and 50 vacancies; however, phase transitions are much sharper for the latter cases. This indicates a unique nature of phase transition in the defective structure with 100 vacancies, dramatically different from the cases with fewer vacancies.

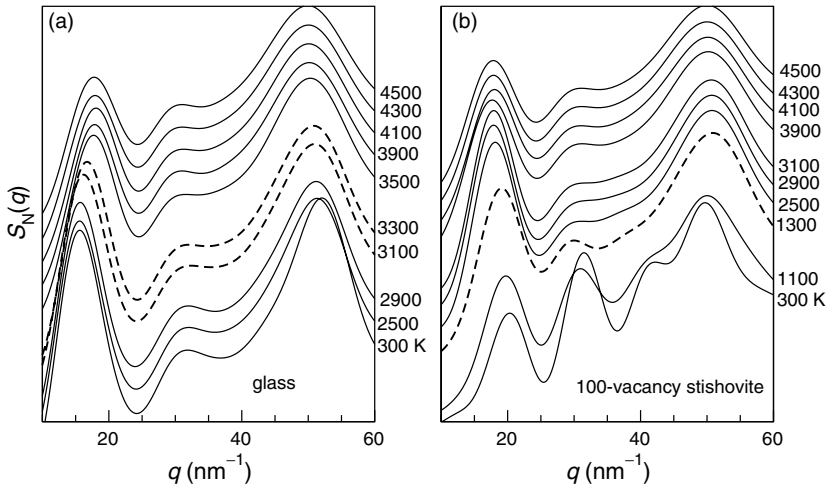

Figure 4. Simulated neutron scattering structure factor: melting of silica glass (a), and solid-state disordering–melting of stishovite with 100 vacancies (b). Dashed curves denote transitional states.

The density, diffusion coefficient, and static structure properties (figures 2–5) reveal that all the structures stay ordered until direct melting except for the case of 100 vacancies, for which solid-state disordering occurs at 1300 K and melting at 3100 K as indicated by the values of D (figure 3). In other words, the defective structure initially with 100 vacancies undergoes two phase transitions (solid-state disordering and melting), and all the other stishovite models experience only melting. At a given temperature, D of the liquids formed from the defective and defect-free structures is nearly identical at the same temperatures, and also agrees with the molten glass (figure 3). We cooled liquid incrementally from 4700 to 3100 K, and found that D is in excellent agreement with the values for the case of 100 vacancies at the same temperatures. In contrast, the disordered solid at 1300 K (initially with 100 vacancies) is in the solid state with D typical of solid and glass (on the order of 10^{-11} m^2 s^{-1}; figure 3). Thus, solid-state disordering of stishovite requires sufficient initial concentration of defects. Defects also enhance melting: the temperature at melting decreases with increasing vacancy concentration as shown in the cases of 0, 1, 2, 10, 20 and 50 vacancies (figures 2 and 3).

The structure evolution and phase transitions in the case of 100 vacancies are interesting for solid-state disordering and melting. Upon heating, the BAD of ∠O–Si–O near 90° (characteristic of SiO_6 octahedra) shifts toward high angles (∼107° at 2900 K, characteristic of SiO_4 tetrahedra), and similarly for the second peak of the BAD of ∠Si–O–Si. Disappearance of the first peak in the BAD of ∠Si–O–Si is more diagnostic of the SiO_6-to-SiO_4 transition where the peak of the Si-ring size distribution shifts from 4 to 6 or 7 (figure 5). Major changes in BAD and the ring-size distribution occur at 1300 K. The structure change is also evident in $S_N(q)$ (figure 4(b)). The pronounced changes in $S_N(q)$, BAD and the ring-size distribution at 1300 K clearly indicate a phase transition: solid-state disordering. The disordered structure evolves into predominantly tetrahedral dense vitreous silica (e.g. near 2500 K). $S_N(q)$ varies slightly with further heating (figure 4(b)). However, we identified a disordered solid–liquid transition at 3100 K where D increases by an order of magnitude from 2900 K. Note that such melting transition is (quasi-)continuous without appreciable structure and density discontinuities.

In contrast to the disordered solid–liquid transition of the defective stishovite structure with 100 vacancies, the melting transition of ordinary vitreous silica glass is still first order

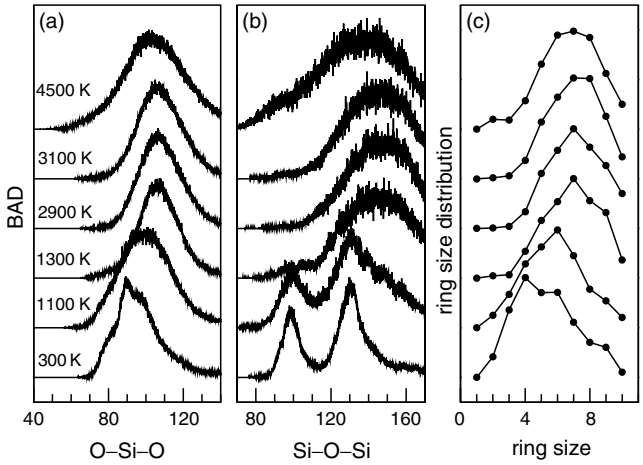

Figure 5. Bond-angle and ring size distributions upon heating of stishovite with 100 removed randomly out of 720 SiO_2 units. The curves were normalized respectively to their peak values and shifted for clarity.

in spite of its sluggishness (figures 2 and 3): the transition begins at 2900 K and completes at 3500 K with an increase in density of about 13% and in D of two orders of magnitude. The transitional nature at 3100 and 3300 K is manifested in density (figure 2) as well as structure features, e.g. the first sharp diffraction peak (FSDP) in $S_N(q)$ (figure 4(a)). FSDP is characteristic of the medium-range order of disordered materials. The shift of FSDP toward higher q is consistent with the density increase of glass during melting, opposite to solid-state disordering of stishovite with 100 vacancies. As shown in figures 4 and 5, the structure formed via solid-state disordering (e.g. stishovite with 100 vacancies at 2900 K) is dominated by the features of SiO_4, thus it can be regarded as a high-density vitreous silica phase compared to ordinary glass at the same temperature. This density excess is a result of solid-state disordering, and explains the (quasi-)continuous melting observed (figure 2).

3.2. Free surfaces: clusters

Free surfaces are ubiquitous for real solids. But chemically metastable stishovite synthesized in a high-pressure press [7] (μm grain size) is effectively stable at ambient conditions. Clusters (e.g. diameter $>$ 5 nm) can also be stable, although there are certainly disordered atoms near the free surfaces. However, the increase of surface-area-to-volume ratio by reducing the cluster size induces complete spontaneous disordering (solid state) at 300 K [18]. Here we explored briefly the disordering process of clusters upon heating and the anisotropy in disordering.

As an example, we conducted constant volume–constant temperature simulations on a cluster with a diameter of 5 nm, and the stress was zero. At 300 K, the cluster is stable at the simulation timescales and manifests the structure features mostly of stishovite, with Si^{VI}/Si of about 0.63 (figures 1 and 6). (Si^{VI}/Si refers to the number ratio of the sixfold coordinated Si to the total Si atoms.) The extent of disordering increases upon increment heating. At 2700 K, the stishovite kernel still exists ($Si^{VI}/Si \sim 0.24$) and the stishovite features are evident in BAD, ring-size distribution and visualization, where the features of disordering become appreciable (figures 1 and 6). At 2900 K, the cluster becomes completely disordered; and further heating induces melting.

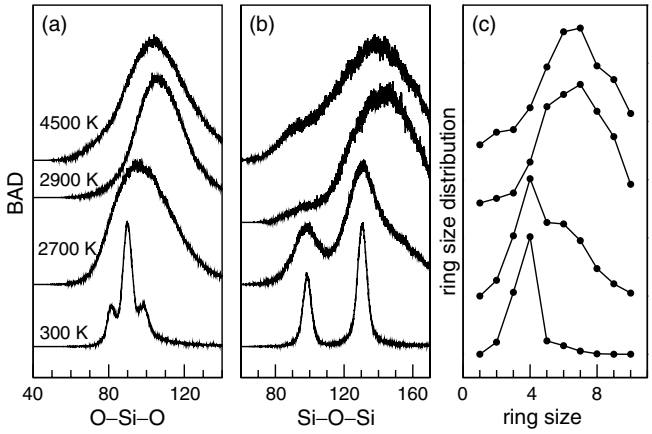

Figure 6. Bond-angle and ring size distributions for the cluster with a diameter of 5 nm upon heating. The curves were normalized respectively to their peak values and shifted for clarity.

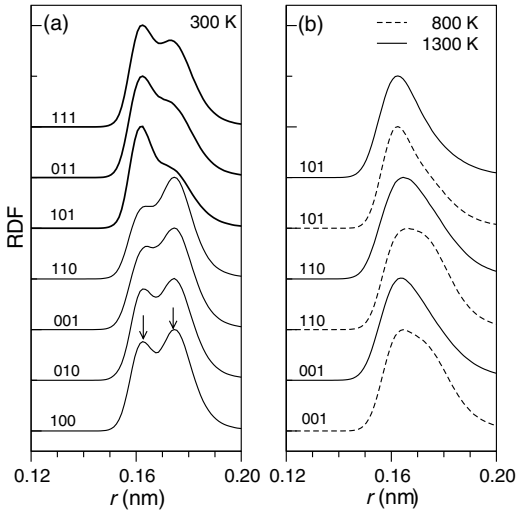

Figure 7. Total radial distribution function (RDF in Si–O regime) for half-clusters with various cutting planes at 300 K (a) and high temperatures (b). The left and right arrows denote peaks due to the contributions of Si^{IV} and Si^{VI}, respectively. Such distinction between the peaks becomes diffusive at high temperatures (b).

The anisotropy of disordering has been reported by Brazhkin *et al* [9] in Raman experiments: disordering occurs more rapidly on the (110) than (001) crystallographic planes. We investigated the anisotropic behaviour using semi-clusters (figure 1(c)) cut from the 5 nm cluster along seven representative crystallographic planes: (100), (010), (001), (110), (101), (011) and (111). While disordering on the semi-sphere is expected to be isotropic, disordering on the cutting plane may depend on its orientation. The sharp corner regime between the semi-sphere and the cutting plane tends to become round to lower free energy, and manifests more pronounced disordering. However, the anisotropic behaviour in disordering on various cutting planes is evident from atomic visualization and structure properties. The first peaks (Si–O) in the RDF at 300 K for the semi-clusters with different cutting planes demonstrate double

peaks or a peak and a shoulder (figure 7), with Si^{IV} in the disordered surface area contributing to the left peak/shoulder, and Si^{VI} in the stishovite kernel to the right. (The presence of Si^{V} as well as homogenization diffuses the peaks.) The relative height of the Si^{IV} and Si^{VI} peaks qualitatively represents the relative amounts of Si^{IV} and Si^{VI}. At 300 K, disordering is anisotropic: it is more pronounced on (101), (011) and (111) than on (100), (010), (001) and (110) planes (figure 7(a)). Upon heating (figure 7(b)), the peak position is closer to the Si^{IV} end for (101) than (110) and (001). Nonetheless, the anisotropy at high temperatures appears less pronounced than at 300 K, possibly due to the half sphere where isotropic disordering smears the feature of the disordering anisotropy along the cutting plane in the gross RDF.

Thus, there is indeed an anisotropy in disordering along different crystallographic planes as suggested previously [9]. However, we observed that disordering on (110) is similar to, but not more pronounced than, (001). Possibly, certain pre-existent defects near the (110) plane may have contributed to its more pronounced disordering inferred in Raman experiments [9].

4. Conclusion

We have investigated disordering of defective stishovite using molecular dynamics simulations. The defects investigated include grain boundaries, vacancies and free surfaces. Solid-state disordering as well as melting is initiated or facilitated by various defects. As an illustrative example, vacancy-rich stishovite transforms into high-density vitreous silica via solid-state disordering prior to (quasi-)continuous melting. Such melting behaviour is in sharp contrast to the sluggish yet first-order melting of glass subjected to the same heating rate. Disordering on free surfaces is anisotropic, being more pronounced along (101), (011) and (111) than (100), (010), (001) and (110) crystallographic planes.

Acknowledgments

This work was partly sponsored by the Inertial Confinement Fusion program at LANL, and performed under the auspices of the US Department of Energy under contract No W-7405-ENG-36.

References

[1] Stishov S M and Popova S W 1961 *Geochem. Int.* **10** 923 (Engl. Transl.)
[2] Skinner B J and Fahey J J 1963 *J. Geophys. Res.* **68** 5595
[3] Hemley R J, Jephcoat A P, Mao H K, Ming L C and Manghnani M H 1988 *Nature* **334** 52
[4] Grimsditch M, Popova S, Brazhkin V V and Voloshin R N 1994 *Phys. Rev.* B **50** 12984
[5] Leger J M, Haines J, Schmidt M, Petitet J P, Pereira A S and de Jornada J A H 1996 *Nature* **383** 401
[6] Andrault D, Fiquet G, Guyot F and Hanfland M 1998 *Science* **282** 720
[7] Luo S N, Mosenfelder J L, Asimow P D and Ahrens T J 2002 *Geophys. Res. Lett.* **29** 1691
[8] Shieh S R, Duffy T S and Li B S 2002 *Phys. Rev. Lett.* **89** 255507
[9] Brazhkin V V, McNeil L E, Grimsditch M, Bendeliani N A, Dyuzheva T I and Lityagina L M 2005 *J. Phys.: Condens. Matter* **17** 1869
[10] Robie R A, Hemmingway B S and Fisher J R 1979 *Thermodynamic Properties of Minerals and Related Substances at 298.15 K and 1 Bar (*10^5 *Pascals) Pressure and at Higher Temperatures* (Washington, DC: US Goverment Printing Office)
[11] Chao E C T, Fahey J J, Littleb J and Milton D L 1962 *J. Geophys. Res.* **67** 419
[12] Endo S, Akai T, Akahama Y, Wakatsuki M, Nakamura T, Tomii Y, Koto K, Ito Y and Tokonami M 1986 *Phys. Chem. Minerals* **13** 146
[13] Tse J S and Klug D D 1991 *Phys. Rev. Lett.* **67** 3559
[14] Tse J S, Klug D D and Page Y L 1992 *Phys. Rev.* B **46** 5933

[15] Trachenko K and Dove M T 2002 *J. Phys.: Condens. Matter* **14** 7449
[16] Badro J, Barrat J L and Gillet P 1996 *Phys. Rev. Lett.* **76** 772
[17] Wentzcovitch R M, da Silva C, Chelikowsky J R and Binggeli N 1998 *Phys. Rev. Lett.* **80** 2149
[18] Luo S N, Zheng L Q and Tschauner O 2005 *Solid State Commun.* **136** 71
[19] Zheng L Q, Lambropoulos J C and Schmid A W 2004 *J. Non-Cryst. Solids* **347** 144
[20] Luo S N, Çağin T, Strachan A, Goddard W A III and Ahrens T J 2002 *Earth Planet. Sci. Lett.* **202** 147
[21] van Beest B V H, Kramer G J and van Santen R A 1990 *Phys. Rev. Lett.* **64** 1955
[22] Saika-Voivod I, Sciortino F and Poole P 2000 *Phys. Rev.* E **63** 011202
[23] Essmann U, Perera L, Berkowitz M L, Darden T, Lee H and Pedersen L G 1995 *J. Chem. Phys.* **103** 8577
[24] Rapaport D C 1995 *The Art of Molecualr Dynamics Simulation* (Cambridge: Cambridge University Press)
[25] Allen M P and Tildesley D J 1987 *Computer Simulation of Liquids* (Oxford: Clarendon)
[26] Voronoi G 1908 *J. R. Angew. Math.* **134** 198
[27] Li J 2003 *Modell. Simul. Mater. Sci. Eng.* **11** 173
[28] Vink R L C and Barkema G T 2003 *Phys. Rev.* B **67** 245201
[29] Nosé S 1984 *J. Chem. Phys.* **81** 511
[30] Parrinello M and Rahman A 1981 *J. Appl. Phys.* **52** 7182
[31] Refson K 2001 *Moldy User's Manual* (Oxford: Department of Earth Sciences)
[32] Gutiérrez G 2002 *Phys. Rev.* B **65** 104202
[33] Hammouda B 1995 *A Tutorial on Small-Angle Neutron Scattering from Polymers* (Gaithersburg: National Institute of Standards and Technology)
[34] Yuan X and Cormack A N 2002 *Comput. Mater. Sci.* **24** 343
[35] Luo S N, Ahrens T J, Çağin T, Strachan A, Goddard W A III and Swift D C 2003 *Phys. Rev.* B **68** 134206
[36] Luo S N, Strachan A and Swift D C 2004 *J. Chem. Phys.* **120** 11640